Digital Elevation Model generation using ascending and Descending multi-baseline ALOS/PALSAR radar images

Jung Hum YU[1], and Linlin GE. Australia

Key words: Digital elevation model, Multi-pass InSAR, DEM merging, Ascending and Descending orbit InSAR.

SUMMARY

Satellite remote sensing can be an efficient and cost-effective technology for acquiring up-to-date and relatively accurate land cover and topographic information. Radar interferometry is a remote sensing technique that can measure high resolution topographic profiles of the Earth's surface. One of the most important applications of the Interferometric Synthetic Aperture Radar (InSAR) technique is the extraction of three-dimensional information from radar images of the Earth's surface. InSAR digital elevation model (DEM) generation relies on the measurement of phase difference between the two sets of complex radar signals, i.e. the range difference between the satellite-borne radar instrument and the ground targets reflecting the radar transmissions. In InSAR DEM generation, the so-called "master image" parameters, such as signal wavelength, incidence angle, and SAR image relationship (i.e. perpendicular baseline), affect the final DEM products. Furthermore, the orbit direction (ascending or descending) provides a different representation of terrain over the same target area. Hence, using images collected by the satellite sensor from different orbit directions is way of improving the quality of InSAR-generated DEMs. The authors propose a combination of two methods to improve DEM quality: firstly, DEM averaging based on the same orbit direction but multi-perpendicular baseline, and secondly, merging the DEMs generated from images collected from different orbit directions in the area of overlap between the radar images.

Digital Elevation Model generation using ascending and descending multi-baseline ALOS/PALSAR radar images

Jung Hum YU[1], and Linlin GE. Australia

1. INTRODUCTION

A digital elevation model (DEM) consists of terrain elevations for ground positions at regularly spaced horizontal intervals. DEMs can be used, for example, in the generation of three-dimensional graphics displaying terrain slope, aspect, and terrain profiles between selected points. DEMs have become an important source of topographical data for many scientific and engineering uses, such as hydrological and geological studies, infrastructure planning and environmental applications. Where topographical data is unavailable, global coverage elevation data sets, typically DEMs from remotely sensed data can be the main source of information. DEM generation techniques and DEM quality assessment includes applications in difficult environments, such as pre- or post-earthquake events and volcanoes (e.g., d'Ozouville et al. 2008; Hirano et al. 2003; Wang et al. 2007).

Remote sensing techniques are a more rapid means of acquiring elevation information over extensive terrain. In particular, processing remotely sensed data collected by earth observation satellites is a very efficient and cost-effective means of acquiring up-to-date and relatively accurate land cover and topographic information. Topographic information has an especially important role to play in Geographic Information Systems (GIS) and in a variety of remote sensing applications. For example, for environmental modelling, resource management, land usage, civil planning or land classification exercises, DEMs are essential. DEMs can be generated using different techniques and from different data sources, including ground survey and levelling, photogrammetry, optical remote sensing, radar, and laser scanning. In the radar case, the two most common methods for generating DEMs from Synthetic Aperture Radar (SAR) images are: (1) radargrammetry, derived from photogrammetry, based on the stereoscopic method, and (2) interferometry, based on the phase differences between identical imaged points in two SAR images. Elevation accuracy varies considerably depending on the method used and the type of environment (e.g. Bourgine & Baghdadi 2005; Ge et al. 2007; Janssen et al. 2004).

Repeat-pass satellite SAR interferometry (InSAR) is a useful method for low-cost, relatively precise and wide-coverage surface DEM generation. The technique involves interferometric phase comparison of two SAR images acquired at different times and with different perpendicular baselines (i.e. different orbit position), and can provide DEMs with metre-level accuracy. InSAR is a technique for extracting three-dimensional information on the terrain topography from the phase "interferograms" of two SAR data images (Ferretti et al. 2001). However, single-baseline and same-orbit direction InSAR systems suffer from the conflict between height sensitivity and interferometric phase aliasing, and geometric effects (Zhenfang et al. 2007). Geometric effects such as layover, foreshortening, and shadowing can be overcome using ascending and descending satellite orbit image pairs.

The ascending-descending orbit combination approach for DEM generation is a very promising technique which can be used to fill in some of the information or elevation gaps in the DEMs caused by the geometric effects. Furthermore, the DEM parameters which are generated by InSAR processing are depending on the master image parameters. So, the InSAR DEMs which are generated with different master images have different grid size and grid location. Moreover, each pair of images has different perpendicular baseline and acquisition conditions (such as water vapour error and noise). In addition, the overlapping of the different DEMs increases the terrain detail and reduces the vertical errors. The authors propose a combination method that: (1) averages DEMs generated using same orbit direction SAR images (with different perpendicular baselines), and (2) then merges the different orbit direction InSAR-generated DEMs in the area of overlap between the SAR imageries.

2. DIGITAL ELEVATION MODEL GENERATION

2.1 DEM generation using InSAR

Synthetic Aperture Radar (SAR) is an active microwave sensor technology developed in the 1950s. With the advantages of consistent multi-temporal image acquisition that is independent of weather conditions and solar illumination, SAR has become an important satellite remote sensing technique, especially in those regions where it is difficult for optical sensors to collect high quality imagery, such as cloud-prone and heavy rain areas as well as in the polar regions. Imaging Interferometric SAR (InSAR) combines complex images recorded either by two satellite antennas at different locations at the same time, or with the same antenna at two different times of satellite overpass. If the same antenna is used at two different times, in the co-called repeat-pass mode, then the location difference (or "perpendicular baseline") must be comparatively small, typically less than a kilometre. The phase difference information between the SAR images is used to measure precise changes in the range or distance, at the radar signal sub-wavelength scale, from the antenna locations to the corresponding point in an image pair. Analysis of the differential phase, and therefore change in distance, between the corresponding pixel centres and the observing antennas can provide information on terrain elevation or, with observations by the same antenna at different times, on terrain displacement (Toutin & Gray 2000).

Before outlining the processing stages for repeat-pass InSAR, it is important to understand the geometric relationships for interferometry of processing images. The imaging geometry of the first pass must be repeated almost exactly in the second pass (He et al. 2007).

In figure 1, H is the altitude of the imaging satellite and R_1, R_2 are the distance between the target on the ground and satellite antennas A_1 and A_2, and B_s is the distance between the antennas A_1 and A_2 at the two satellite imaging locations.

In a single SAR image, a pixel's phase information can not be used. However, the differential phase from two independent SAR satellite images of the same ground pixel target contains useful 3D-terrain information. The SAR images have a spatial resolution defined by the pulse length, altitude of the satellite and look angle. The slant range resolution is ½ the

pulse length. The ground range resolution is defined as the slant range resolution divided by the cosine of the look angle. The SAR images are usually selected for the same area based on the two adjacent-pass orbits (i.e. short "temporal baseline"), and the set of phase differences for all pixels of the two SAR images is used to generate the interferogram. The SAR phase is derived from complex SAR images.

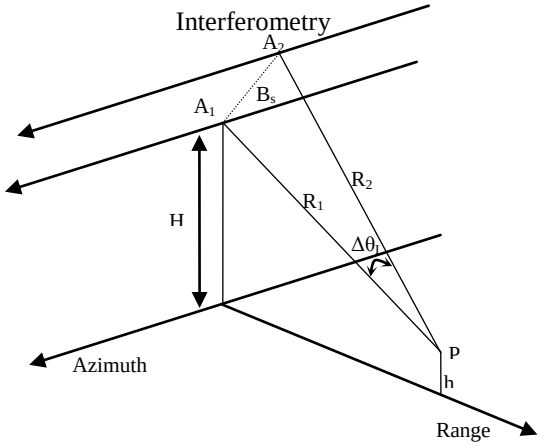

Figure 1: Geometry of Interferometric SAR (InSAR)

InSAR digital elevation model generation is based on the processing of at least two complex SAR images covering the same area and acquired from slightly different points of view (e.g. Crosetto 2002; Zhou et al. 2005). The elevation information is obtained from the interferogram by "unwrapping" the interferometric phases (e.g. Ferretti et al. 1999).

The interferometric phase can be written as

$$\phi = \phi_{flat} + \phi_{topo} + \phi_{defo} + \phi_{atm} + \phi_{noi} \quad (1)$$

where ϕ is the interferometric phase, ϕ_{flat} is the flat earth phase, ϕ_{topo} is the topographic phase, ϕ_{defo} is the deformation phase, ϕ_{atm} is the atmospheric delay phase and ϕ_{noi} is the noise.

In equation (1), the "flat earth" phase ϕ_{flat} and noise ϕ_{noi} can be removed by using the orbit information correction and applying an interferogram filtering method. When the imaging interval is sufficiently short, there is no deformation phase ϕ_{defo}. If the atmospheric delay phase ϕ_{atm} can be ignored, then equation (1) reduces to:

$$\phi = \phi_{topo} \quad (2)$$

The DEM is obtained by "unwrapping" the phase ϕ and converting the phase to a height quantity for the pixel, and then geo-coding the pixel. The coordinate and each parameter of the InSAR DEMs are determined according to the parameters of the master image (Ferretti et al 2001).

Figure 3 shows the flowchart of DEM generation using the repeat-pass InSAR technique. Externally-derived DEMs are used for reducing the errors in data processing (Zhou et al. 2005).

2.2 Ascending and descending InSAR

A satellite can acquire an image when it passes from south to north (ascending orbit) or north to south (descending orbit). Images from ascending and descending orbits have different imaging geometry. Due to the structure of the SAR signal transmitter and receiver, the SAR image consists of slant ranges. This characteristic of a SAR image is a limitation of image acquisition, especially for the extraction of terrain information due to problems with foreshortening, layover and shadow areas. In the case of foreshortening, the ground resolution is slightly degraded, although the heights can still be calculated. However no information can be recovered if there is layover or shadowing. If both ascending and descending passes are used, foreshortening, layover and shadowing in one orbit direction's InSAR pair may be recovered from other passes (Crosetto 2002; Yun et al. 2006).

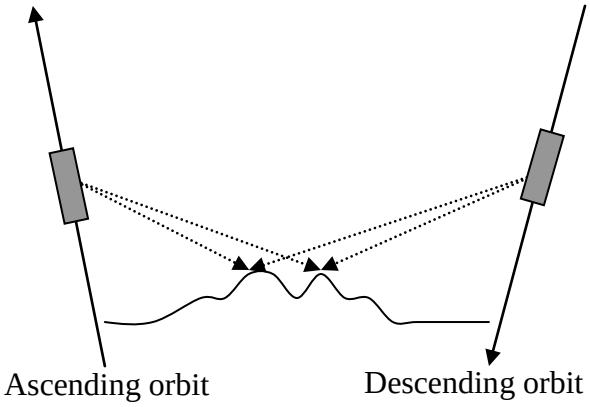

Figure 2: Geometry of ascending and descending SAR imaging.

2.3 Methodology

In this paper an external DEM, in contrast to the conventional InSAR method for DEM generation is used to generate the known topographic phase which is then subtracted from the interferogram. Each SAR image is in the format of Single Look Complex (SLC) files, containing both amplitude and phase information of the backscattered signal from the ground surface. These two SAR images have to be coregistrated pixel-by-pixel. The simulated SAR image is generated for use in coregistration of the external DEM to the master image. The remaining phase, which is the height difference with respect to the external DEM, is removed for phase unwrapping, and the unwrapped phase is converted to a height map. Image pairs (master and slave) are selected to have as short a temporal baseline as possible, in order to increase the degree of coherence.

Interferometric processing requires a comparatively short temporal baseline between image acquisitions in order to ensure maximum coherence between acquisitions (e.g. d'Ozouville et al. 2008; Rabus et al. 2003; Sandwell et al. 2008).

The basis of InSAR processing for DEM generation is the phase measurement, and the conversion of phase to height (Zhou et al. 2005). The height sensitivity of interferometric phase is defined as:

$$\frac{\Delta\phi}{\Delta h} = -\frac{4\pi}{\lambda}\frac{B\cos(\theta-\alpha)}{R\sin\theta} = -\frac{4\pi}{\lambda}\frac{B_{\perp}}{R\sin\theta} \tag{3}$$

where B is the baseline, θ is the side looking angle, α is the baseline tilt angle, λ is the wavelength, R is the distance between the scatter and the radar antenna, and $B_{\perp}$ is the perpendicular baseline.

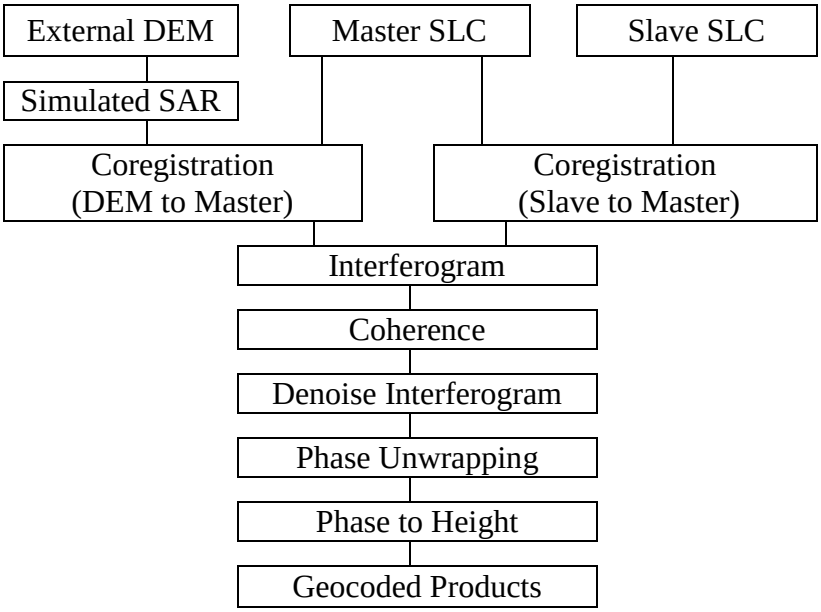

Figure 3: The flow chart of InSAR DEM generation

The altitude of ambiguity (h_a) is defined as the altitude difference that generates an interferometric phase change of 2π after interferogram flattening. The altitude of ambiguity is inversely proportional to the perpendicular baseline:

$$h_a = \frac{\lambda R\sin\theta}{2B_{\perp}} \tag{4}$$

As the baseline increases, the altitude of ambiguity decreases, which corresponds to an increase in the topographic sensitivity of the interferogram. Each data pair has a different perpendicular baseline and slightly different orbit and look angle. This means that each interferogram, generated by different pairs of SAR images, have specific fringe patterns for the same target terrain. In the phase unwrapping step, various fringe patterns affect the processing difficulty and sensitivity of the derived DEM differently. Therefore, DEMs processed with different perpendicular baseline pairs can fill in the height gap of other DEMs (Massonnet & Feigl 1998).

2.4 InSAR DEM merging

Figure 4 shows how the reconstructed DEM using a different master image fills in the gaps in other DEMs. This interpolation is affected by the perpendicular baseline and the slightly different orbit for each master image.

Parameters of the InSAR-generated DEMs are affected by the master image parameters. Even if the master and slave images are swapped slightly different DEMs are generated. Therefore, each InSAR-generated DEM generated by different master images have different grid location and altitude of ambiguity. These factors provide the different elevation contour and grid density.

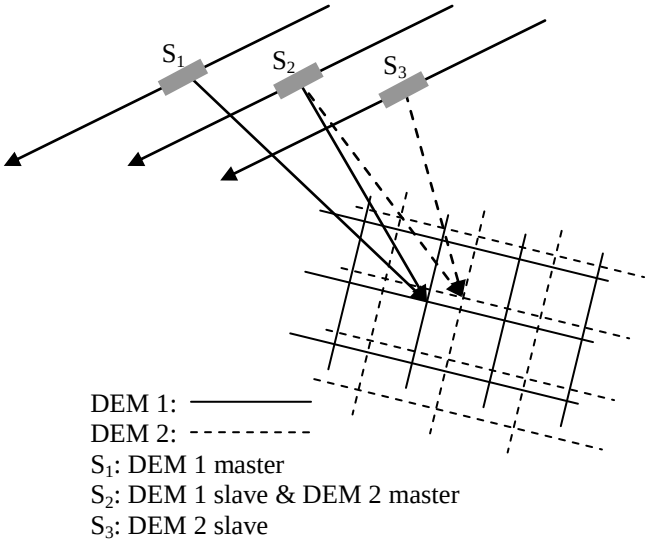

Figure 4: Different grid location using different master images

3. EXPERIMENTAL RESULT

3.1 Ascending and descending SAR images

The test site is the Appin area in the state of New South Wales, Australia. This research used the ascending and descending ALOS/PALSAR SAR images (L-band) to generate the DEMs. The LiDAR-generated DEM is used as the reference or "ground truth" DEM. Table 1 summarises the SAR data information. The ascending pairs correspond to 1-repeat cycle (46 days) and 2-repeat cycle orbits, while the descending pairs are from 1-repeat cycle orbits. In order to improve the coherence of image pairs, short temporal baselines are selected for DEM generation. Perpendicular baseline is selected with reference to 13.1km for ALOS/PALSAR (28MHZ) (Sandwell et al. 2008). Comparing with each baseline of ascending and descending data pairs, descending pairs have similar distance but ascending pairs have different distance. Also, it is good combination for test the relationship of baseline distance and height sensitivity. Figure 5 are intensity images of ALOS/PALSAR pairs over the test site.

Table 1: ALOS/PALSAR data information

Orbit direction	Master date	Slave date	Bperp (m)	Btemp (days)
Ascending	14/11/2007	30/12/2007	757	46
Ascending	31/03/2008	01/07/2008	2992	92
Descending	01/06/2008	17/07/2008	2809	46
Descending	17/07/2008	01/09/2008	2245	46

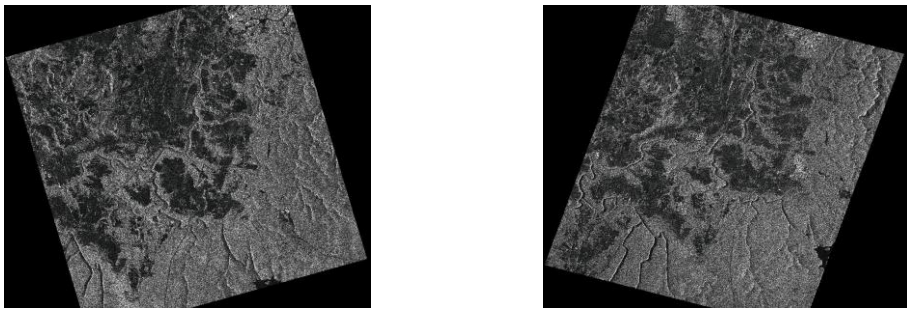

Figure 5: Ascending (14/11/07-30/12/07-left) and descending (31/03/08-01/07/08-right) intensity images for the Appin test site

Figure 6 shows the satellite orbits of the four master SAR images. Ascending and descending orbits have different location. In illustration, the look direction which observes the targets from sensor is opposite direction and if the target area is the mountainous terrain, acquired scattering data has different site of terrain. Furthermore, if the orbit direction is same, the perpendicular baseline between the each sensor is small compered with the sensor from the opposite orbit direction. Table 2 contains the coordinates of the SAR sensor at master image acquisition.

Table 2: Sensor coordinates of master image acquisition.

14/11/07 (ascending)	31/03/08 (ascending)	01/06/08 (descending)	17/07/08 (descending)
x: -2856373.802094	x: -3040335.831031	x: -6707162.857529	x: -6701692.082298
y: 1097104.822033	y: 1279255.936505	y: 1899414.157338	y: 1904276.312634
z: -6385403.343382	z: -6265549.035622	z: -1218993.206261	z: -1243920.082046
:	:	:	:
x: -4157288.447444	x: -4288210.356967	x: -5877443.151306	x: -5864312.114955
y: 2487202.205073	y: 2652202.757768	y: 2136941.414350	y: 2140731.511050
z: -5163304.559381	z: -4970522.105656	z: -3316185.929882	z: -3338135.812850
x: -4364151.483460	x: -4482810.663974	x: -5636350.780352	x: -5621847.469556
y: 2745951.776000	y: 2905162.523010	y: 2154058.261601	y: 2157551.683165
z: -4851866.984389	z: -4646598.148115	z: -3701880.070780	z: -3722964.365773

x: -4551266.427681 y: 2995398.293813 z: -4520801.568977 : x: -5170285.601537 y: 4063030.309414 z: -2620137.318473	x: -4657235.576525 y: 3148067.603499 z: -4303871.713414 : x: -5208430.981699 y: 4172613.854257 z: -2358835.016940	x: -5372483.374387 y: 2160300.703511 z: -4072572.314679 : x: -3755355.679372 y: 2022833.170602 z: -5651227.321364	x: -5356674.953779 y: 2163474.029433 z: -4092709.654788 : x: -3734200.183358 y: 2024127.196886 z: -5665572.813421
x: -5228035.224469 y: 4233246.960352 z: -2201679.887730	x: -5252162.219761 y: 4332363.981366 z: -1934548.110552	x: -3382228.785101 y: 1961287.918233 z: -5903117.710904	x: -3360268.158141 y: 1962166.015242 z: -5916129.478502
x: -5263305.325485 y: 4386815.161994 z: -1774286.178125	x: -5273405.483688 y: 4474939.420301 z: -1502407.266720	x: -2996130.515500 y: 1888558.360151 z: -6131167.593247	x: -2973460.429460 y: 1889012.695232 z: -6142800.095161

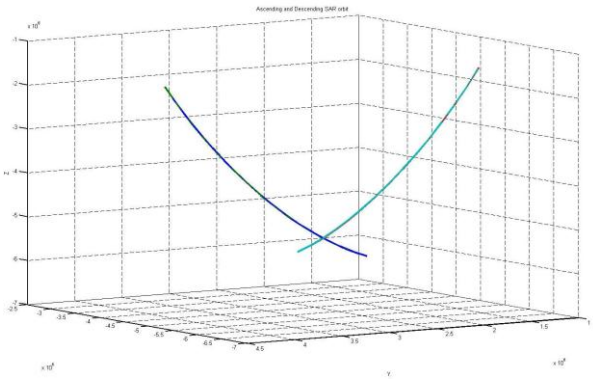

Figure 6: Orbits in ascending and descending directions

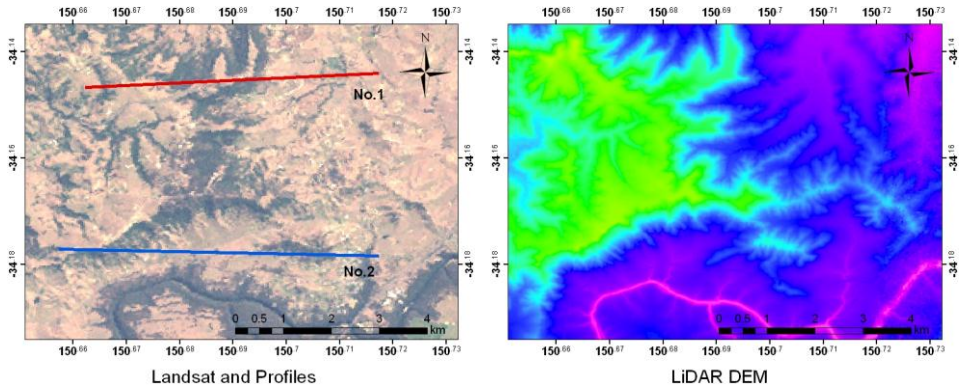

Figure 7: Profile lines (no.1 and 2-left) with Landsat image and LiDAR DEM of the in Appin area

Profile lines was selected for verification of the accuracy of the final DEM (see Figure 7). Profile direction is the same direction as the range direction. Figures 8 and 9 show the InSAR-generated DEM using ALOS/PALSAR images. In figure 8, the short temporal baseline DEM

(14/11/07-30/12/07) appears to have more noise than the longer baseline DEM (31/03/08-01/07/08). It is related with the height sensitivity of interferometric phase. Descending InSAR-generated DEMs have similar perpendicular baseline values.

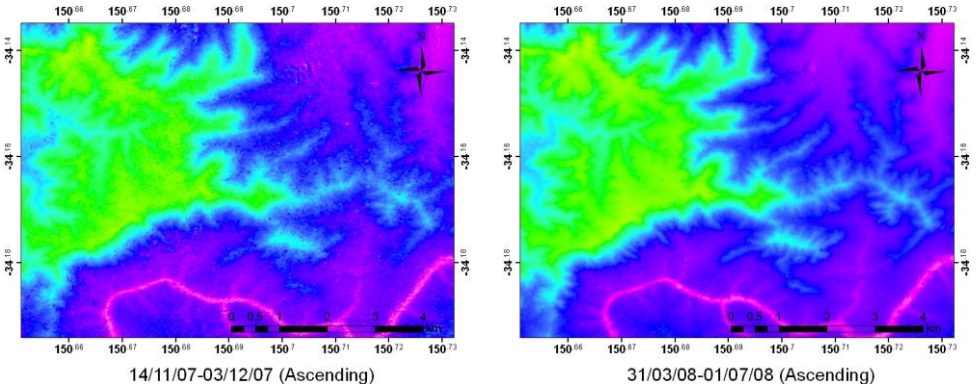

Figure 8: ALOS ascending (14/11/07-30/12/07-left) and ALOS ascending (31/03/08-01/07/08-right) InSAR-generated DEMs.

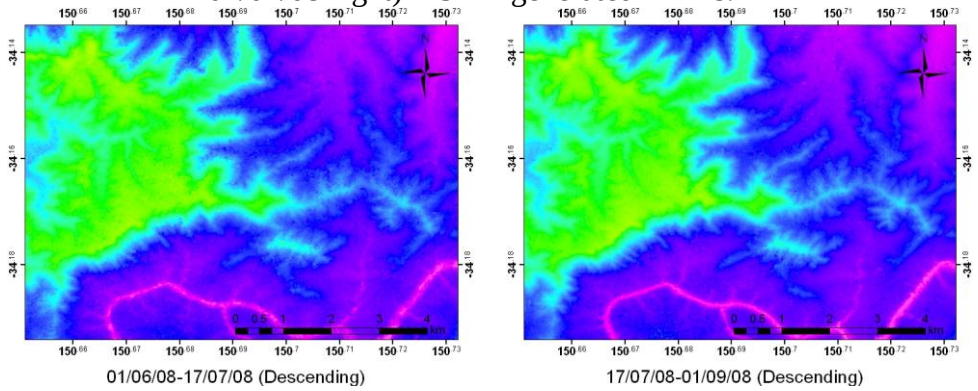

Figure 9: ALOS descending (01/06/08-17/07/08-left) and ALOS descending (17/07/08-01/09/08-right) InSAR-generated DEMs

Figures 10 and 11 show profile line no.1 results from the descending and ascending InSAR DEMs. Both InSAR-generated DEMs have samilar noise patterns in the valley area and on the slopes of the mountain. Because, in the valley area, terrain is ”hidden” from sensor sight and hence the sensor has poor terrain information at both ascending and descending direction. Furthermore, this phenomenon occures on mountain slopes which are located on opposite sides from the sensor. In particular, in the ascending case, terrain distortions or noise appear next to the mountainous area (figure 11, ID: 375~460). This is alos clearly seen in the other profile (no.2, ID:181~253) in figure 13. Generally, a shadow area in the SAR image is non-information area and it is interpolated by surrounded information during the InSAR DEM processing. However, this limitation can be recovered using different site observation. The possibility show in the figures 15 and 16. Comparting with single InSAR DEM and merged InSAR DEM, the elevation errors in the problem area are reduced and the terrain reality is improced by merged technique. In figures 12 and 13, DEM differences along the profiles (no.

1 & 2) are shown. Table 3 gives the RMSE of each DEM derived from a comparison with the reference LiDAR-generated DEM.

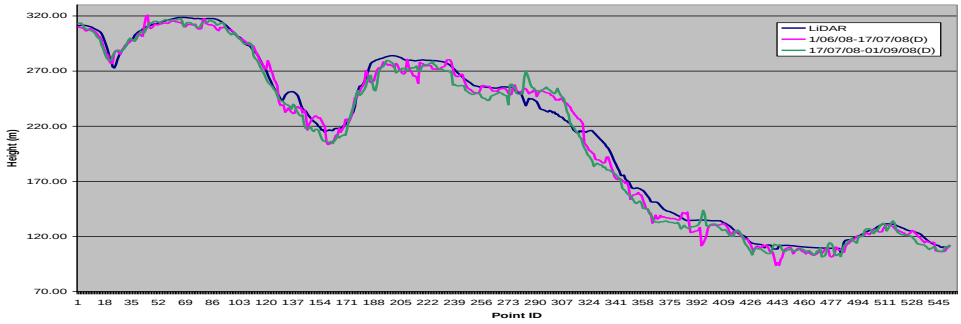

Figure 10: Profile (no.1) of descending InSAR-generated DEMs compared with LiDAR-generated DEM.

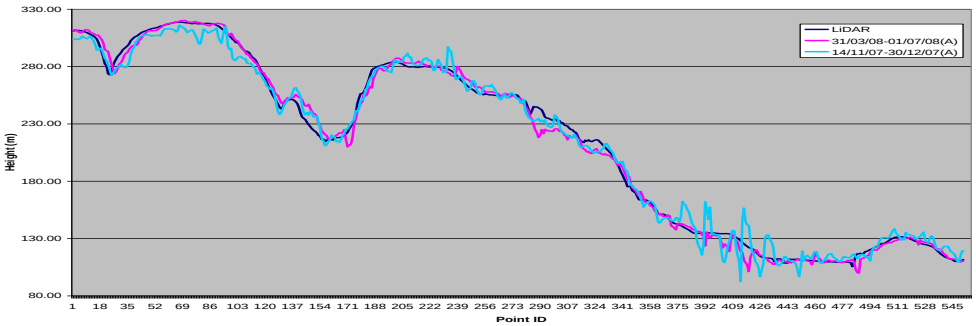

Figure 11: Profile (no.1) of ascending InSAR-generated DEMs compared with LiDAR-generated DEM.

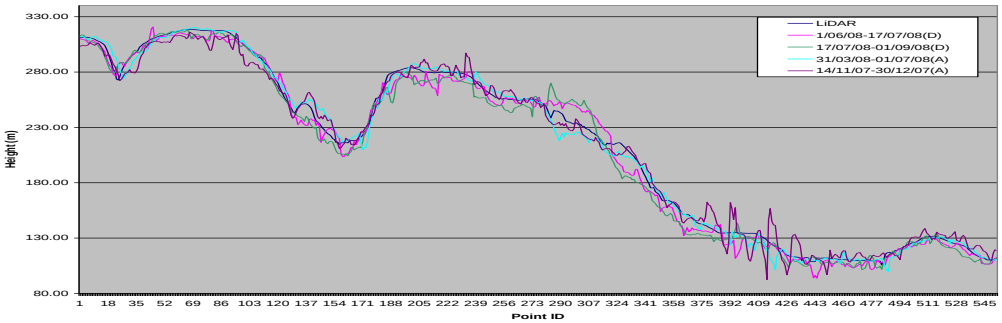

Figure 12: Profile (no.1) of ascending and descending InSAR-generated DEMs compared with LiDAR-generated DEM.

Table 3: Root mean square error of InSAR-generated DEM (in metres).

	1/06/08-17/07/08(D)	17/07/08-01/09/08(D)	31/03/08-01/07/08(A)	14/11/07-30/12/07(A)
No.1	1.74	2.11	0.86	0.76
No.2	1.55	1.89	0.31	1.77

Figure 14 shows the merged InSAR-generated DEM. Asending and descending InSAR-generated DEMs were merged depending on the orbit direction. In the figures 15 and 16 it can be seen that the DEM height variation has been reduced compare with a single InSAR-generated DEM.

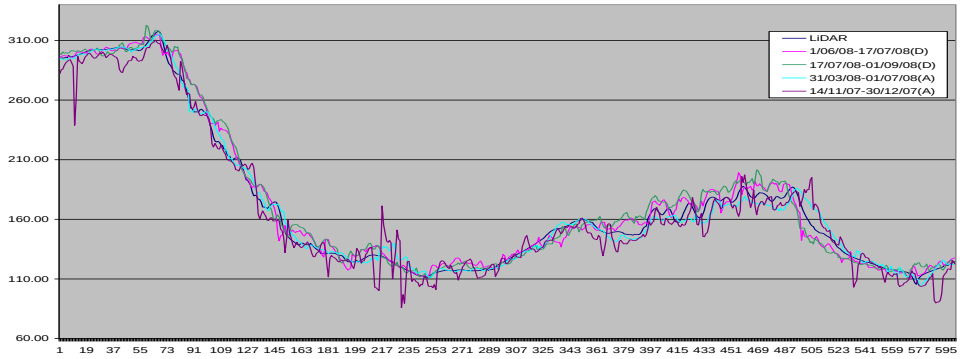

Figure 13: Profile (no.2) of ascending and descending InSAR-generated DEMs compared with LiDAR-generated DEM.

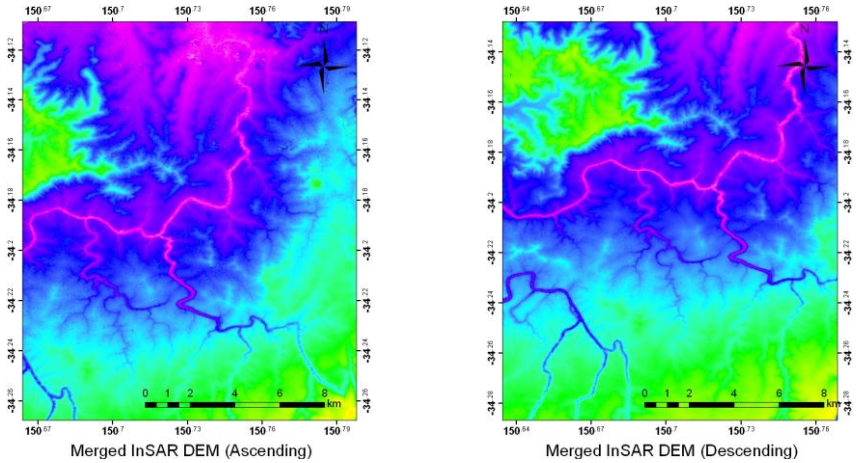

Figure 14: Merged InSAR-generated DEM from asending and descending passes.

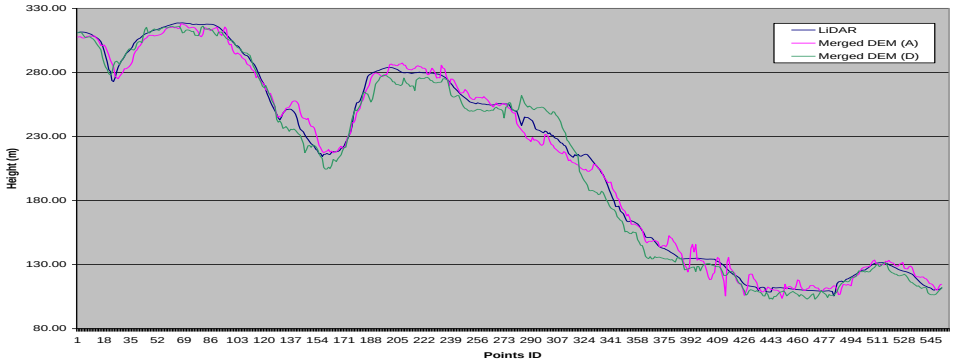

Figure 15: Profile (no.1) of merged (ascending and descending) DEM.

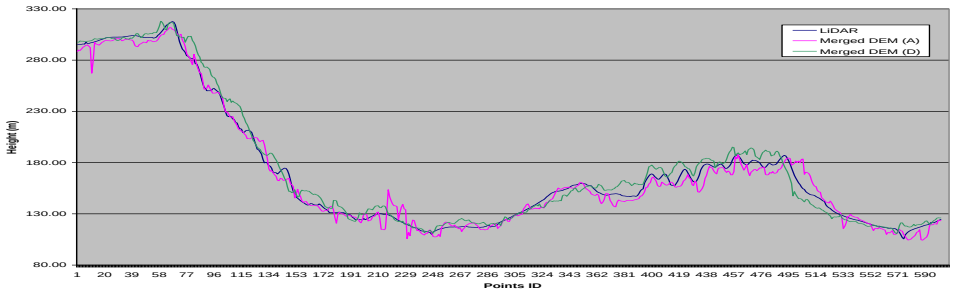

Figure 16: Porfile (no.2) of merged (ascending and descending) DEM

4. CONCLUDING REMARKS

The results reported in this paper are for an area of about 500 km^2 around Appin in the state of New South Wales. Two ascending and descending ALOS/PALSAR image pairs have been used for InSAR DEM generation. One arc second resolution DEM was used as external DEM data to model and remove symmetrical phase errors. For steep slopes and severe changes in topography, the phase unwrapping process was improved by first subtracting the phase calculated from an external DEM. The topographical changes restrict the final DEM accuracy. However, the geometric effects due to the valley and mountain slope are mitigated by using different orbit direction InSAR-generated DEMs. Figures 10 and 11 show the difference of terrain responses by the different sensor orbit direction. The sensor location of the ascending and descending orbit images is located on opposite sides of the target area. Therefore, the terrain representation is different and terrain information is limited. However, the DEM merging method using different orbit direction data can improve the terrain reality and can support the other's data limitation.

The InSAR-generated DEM, generated from the same SAR sensor data, has simular spatial resolution but it does not correspond to exactly the same location because satellite orbit information is different and final products generated using such orbit information have different outcomes. The ascending pair cases are good examples for the comparison of relationship of height sensitivity and perpendicular baseline. A short baseline pair has more noise than long baseline pair and it is one of elevation error of InSAR DEM generation. Therefore, merging method is useful technique for improve the DEM generation. Figure 14 presents that the results of the merged InSAR-generated DEMs, combining same orbit direction InSAR-generated DEMs. This merging method, using different master image DEM, reduces the height errors compared to single InSAR-generated DEMs.

In figure 8, short baseline DEM (14/11/07-30/12/07) has more noise than the long baseline DEM (31/03/08-01/07/08). For the terrain deformation monitoring applications, short perpendicular baselines are preferred. However, for DEM generation, a more suitable baseline is one that is increased because of the effect of base-height ratio and the height sensitivity of interferometric phase. Different orbit direction and merged InSAR-generated DEMs provide the improved quality DEMs

5. REFERENCES

Bourgine, B., & Baghdadi, N., 2005, 'Assessment of C-band SRTM DEM in a dense equatorial forest zone', *Comptes Rendus Geosciences*, 337(14), 1225-1234.

Crosetto, M., 2002, 'Calibration and validation of SAR interferometry for DEM generation', *Journal of Photogrammetry & Remote Sensing*, 57, 213-227.

d'Ozouville, N., Deffontaines, B., Benveniste, J., Wegmuller, U., Violette, S., & de Marsily, G., 2008, 'DEM generation using ASAR (ENVISAT) for addressing the lack of freshwater ecosystems management, Santa Cruz Island, Galapagos', *Remote Sensing of Environment*, 112(11), 4131-4147.

Ferretti, A., Prati, C., & Rocca, F., 1999, 'Multibaseline InSAR DEM reconstruction: the wavelet approach' *IEEE Transactions on Geoscience & Remote Sensing*, 37(2), 705-715.

Ferretti, A., Prati, C., & Rocca, F., 2001, 'Permanent scatterers in SAR interferometry', *IEEE Transactions on Geoscience & Remote Sensing*, 39(1), 8-20.

Ge, L., Chang, H.C., & Rizos, C., 2007, 'Mine subsidence monitoring using multi-source satellite SAR images', *Photogrammetric Engineering & Remote Sensing*, 73(3), 259-266.

He, X., Luo, H., Huang, Q., & He, M., 2007, 'Integration of InSAR and GPS for hydraulic engineering', *Science in China Series E: Technological Sciences*, 50, 11-124.

Hirano, A., Welch, R., & Lang, H., 2003, 'Mapping from ASTER stereo image data: DEM validation and accuracy assessment', *ISPRS Journal of Photogrammetry & Remote Sensing*, 57(5-6), 356-370.

Janssen, V., Ge, L., & Rizos, C., 2004, 'Tropospheric corrections to SAR interferometry from GPS observations', *GPS Solutions*, 8(3), 140-151.

Massonnet, D., & Feigl, K.L., 1998, 'Radar interferometry and its application to changes in the Earth's surface', *Reviews of Geophysics*, 36(4), 441-500.

Rabus, B., Eineder, M., Roth, A., & Bamler, R., 2003, 'The shuttle radar topography mission-a new class of digital elevation models acquired by spaceborne radar', *ISPRS Journal of Photogrammetry & Remote Sensing*, 57(4), 241-262.

Sandwell, D.T., Myer, D., Mellors, R., Shimada, M., Brooks, B., & Foster, J., 2008, 'Accuracy and resolution of ALOS interferometry: vector deformation maps of the Father's

Day intrusion at Kilauea', *IEEE Transactions on Geoscience & Remote Sensing*, 46(11), 3524-3534.

Toutin, T., & Gray, L., 2000, 'State-of-the-art of elevation extraction from satellite SAR data', *ISPRS Journal of Photogrammetry & Remote Sensing*, 55(1), 13-33.

Wang, H., Xu, C., & Ge, L., 2007, 'Coseismic deformation and slip distribution of the 1997 Mw 7.5 Manyi, Tibet, earthquake from InSAR measurements', *Journal of Geodynamics*, 44(3-5), 200-212.

Yun, S., Segall, P., & Zebker, H., 2006, 'Constraints on magma chamber geometry at Sierra Negra Volcano, Galapagos islands, based on InSAR observation', *Journal of Volcanology and Geothermal Research*, 150, 232-243.

Zhenfang, L., Zheng, B., & Zhiyong, S., 2007, 'A joint image coregistration, phase noise suppression and phase unwrapping method based on subspace projection for multibaseline InSAR systems', *IEEE Transactions on Geoscience & Remote Sensing*, 45(3), 584-591

Zhou, C., Ge, L., E, D., & Chang, H.C., 2005, 'A case study of using external DEM in InSAR DEM generation', *Geo-Spatial Information Science*, 8(1), 14-18.

CONTACTS

Mr. Jung Hum Yu[1], and A/Prof. Linlin Ge
School of Surveying and Spatial Information Systems
University of New South Wales
Sydney, NSW
Australia
Tel: +61-2-9385-4201
Fax: +61-2-9313-7493
[1]Jung.yu@student.unsw.edu.au